Correction to: Binary black hole mergers from population III stars: uncertainties from star formation and binary star properties

Filippo Santoliquido, Michela Mapelli, Giuliano Iorio, Guglielmo Costa, Simon C. O. Glover, Tilman Hartwig, Ralf S. Klessen, Lorenzo Merli

Monthly Notices of the ROYAL ASTRONOMICAL SOCIETY

MNRAS **528,** 954–962 (2024) https://doi.org/10.1093/mnras/stad3969
Advance Access publication 2024 January 22

Correction to: Binary black hole mergers from population III stars: uncertainties from star formation and binary star properties

by Filippo Santoliquido [1,2★] Michela Mapelli [1,2,3★] Giuliano Iorio [1,2,3★] Guglielmo Costa [1,2,3,4] Simon C. O. Glover [5] Tilman Hartwig [6,7,8] Ralf S. Klessen [5] and Lorenzo Merli [1]

[1]*Physics and Astronomy Department Galileo Galilei, University of Padova, Vicolo dell'Osservatorio 3, I–35122, Padova, Italy*
[2]*INFN–Padova, Via Marzolo 8, I–35131, Padova, Italy*
[3]*INAF–Osservatorio Astronomico di Padova, Vicolo dell'Osservatorio 5, I–35122, Padova, Italy*
[4]*Univ Lyon, Univ Lyon1, Ens de Lyon, CNRS, Centre de Recherche Astrophysique de Lyon UMR5574, F-69230, Saint-Genis-Laval, France*
[5]*Universität Heidelberg, Zentrum für Astronomie, Institut für Theoretische Astrophysik, Albert-Ueberle-Str. 2, D–69120 Heidelberg, Germany*
[6]*Department of Physics, School of Science, The University of Tokyo, Bunkyo, Tokyo 113-0033, Japan*
[7]*Institute for Physics of Intelligence, School of Science, The University of Tokyo, Bunkyo, Tokyo 113-0033, Japan*
[8]*Kavli Institute for the Physics and Mathematics of the Universe (WPI), The University of Tokyo Institutes for Advanced Study, The University of Tokyo, Kashiwa, Chiba 277-8583, Japan*

Key words: errata, addenda – black hole physics – gravitational waves – methods: numerical – stars: Population III – galaxies: star formation.

Our paper 'Binary black hole mergers from population III stars: uncertainties from star formation and binary star properties' was published in MNRAS, 524, p. 307–324 (2023).

After publication, we found a minor bug in COSMO$\mathcal{R}$ATE, the code we used to produce the results shown in Figs 2, 3, 4, 5, 6, 7, 8, 9, 10, 12, 13, 14, 15, 17, 18, B1, and B2.

In the following, we list the changes with respect to the published version of the paper. All of them are minor changes: the results and conclusions presented in the published article are not significantly affected by the bug.

(i) Figs 2, 3, 4, 5, 6, 7, 8, 9, 10, 12, 13, 14, 15, 17, 18, B1, and B2 should be replaced by those reported in this Erratum.

(ii) The last paragraph of section 3.2 should be replaced by: 'We expect that a large fraction of the detected Pop. III BBH mergers occur at redshift $z > 8$, during or before the cosmic reionization. This value significantly depends on the adopted SFRD model: we estimate that 60–71 per cent detectable Pop. III BBH mergers take place at $z > 8$ according to H22, 66–78 per cent according to SW20, 45–54 per cent with the SFRD by J19, and 28–34 per cent assuming LB20.'

(iii) The second sentence in the second to last paragraph of section 5 should be changed as follows: 'In particular, for our fiducial model (LOG1 with SFRD from H22) we expect ≈530 detections per year, of which 68 per cent from BBH mergers occurring at redshift $z > 8$.'

(iv) The main data presented in this work are publicly available on Zenodo at Santoliquido (2023).

(v) A new version of COSMO$\mathcal{R}$ATE with this bug fixed is publicly available on GitLab at this link.

We apologize for the inconvenience.

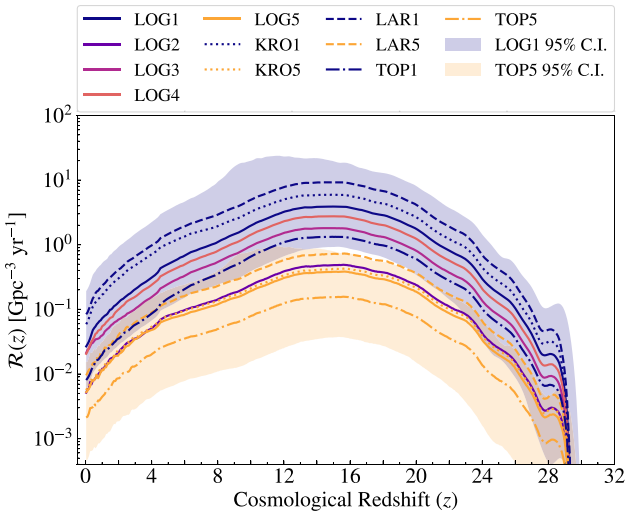

Figure 2. Evolution of the BBH merger rate density with redshift $\mathcal{R}(z)$ assuming the SFRD from H22, and the corresponding 95 per cent credible interval. Solid lines: models with a flat-in-log IMF (LOG). Dotted lines: Kroupa IMF (KRO). Dashed lines: Larson IMF (LAR). Dot–dashed lines: top-heavy IMF (TOP). The shaded areas are 95 per cent credible interval evaluated considering input uncertainty in A-SLOTH (see fig. 1 and section 2.3.1) for the models LOG1 and TOP5.

★ E-mail: filippo.santoliquido@phd.unipd.it (FS); michela.mapelli@unipd.it (MM); giuliano.iorio@unipd.it (GI)

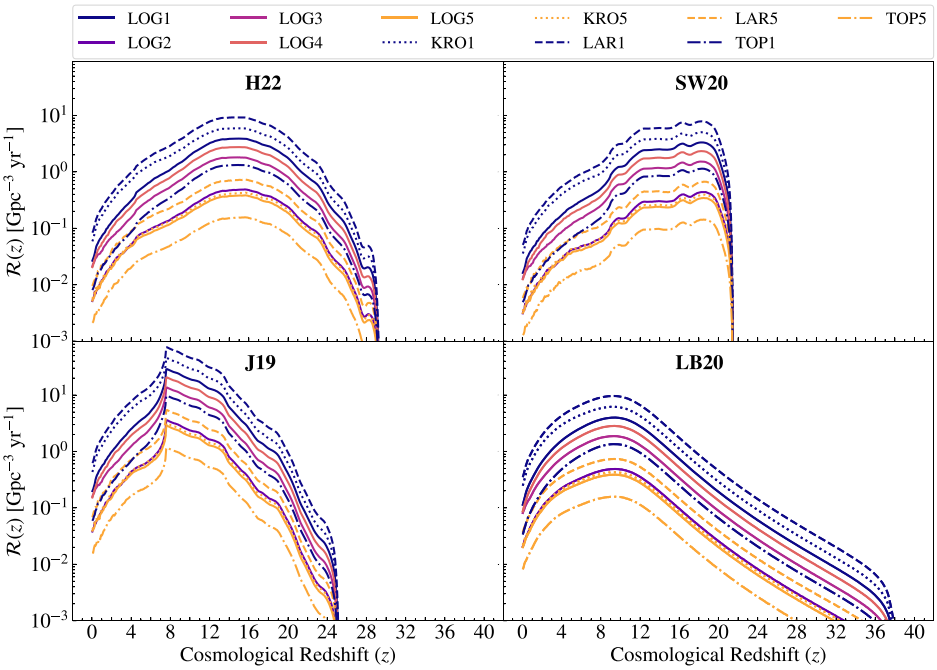

Figure 3. Evolution of the BBH merger rate density with redshift $\mathcal{R}(z)$ for all the 44 models considered in this work. Solid lines: models with a flat-in-log IMF (LOG). Dotted lines: Kroupa IMF (KRO). Dashed lines: Larson IMF (LAR). Dot–dashed lines: top-heavy IMF (TOP). Upper left plot: H22 star formation history, upper right: SW20, lower left: J19, and lower right: LB20.

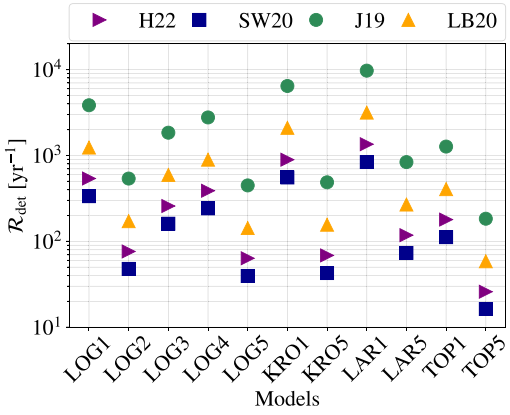

Figure 4. Detection rate $\mathcal{R}_{\rm det}$ of Pop. III BBHs, assuming the Einstein Telescope triangle configuration (ET-D) and $\rho_{\rm th} = 9$. See section 2.5 for details. Purple right-pointing triangles: SFRD from H22; blue squares: SW20; green circles: J19; orange triangles: LB20.

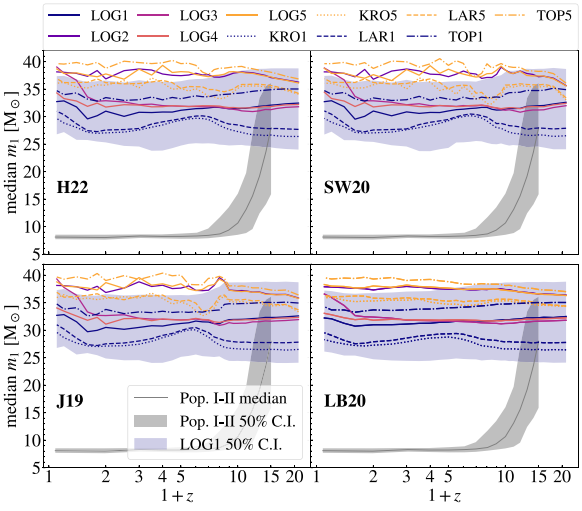

Figure 5. Median primary BH mass m_1 as a function of redshift, for all the models considered in this work. The blue shaded area is the interval from the 25th to the 75th percentile of the primary BH mass distribution at fixed redshift for the LOG1 model. Upper left-hand panel: H22 SFRD model, upper right-hand panel: SW20, lower left-hand panel: J19, and lower right-hand panel: LB20. The grey thin solid line shows the median primary mass of Pop. I-II BBHs in our fiducial model (appendix A). The shaded grey area is the corresponding 50 per cent credible interval.

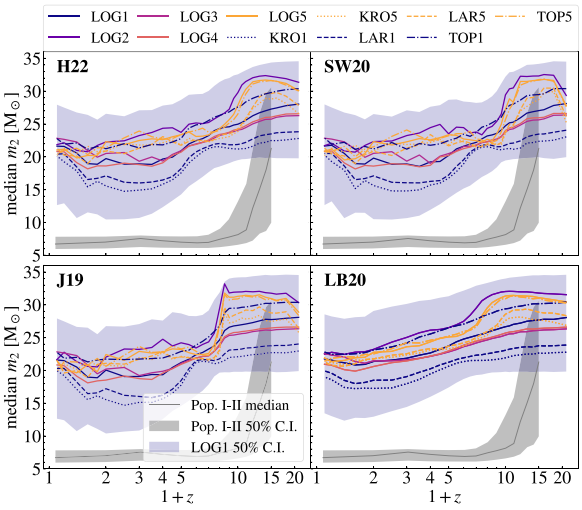

Figure 6. Same as Fig. 5 but for the secondary BH mass m_2.

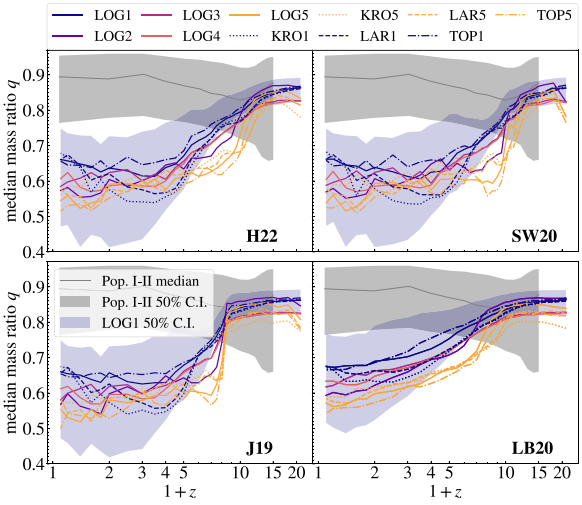

Figure 7. Same as Fig. 5 but for the BH mass ratio q.

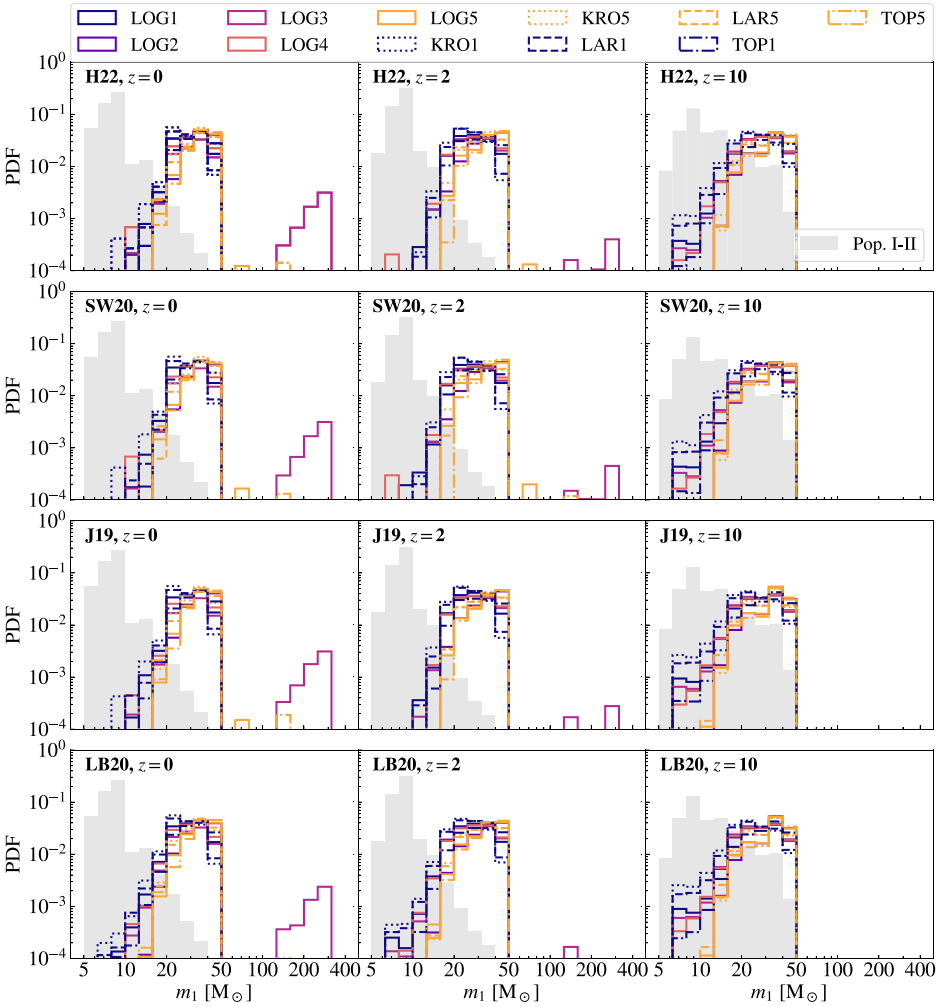

Figure 8. Primary BH mass distribution m_1 for three different redshift bins (from left to right $z = 0$, 2, and 10) and the four SFRD models considered in this work (from top to bottom H22, SW20, J19, and LB20). The grey shaded histograms show the primary mass distribution of Pop. I-II BBHs in our fiducial model (appendix A).

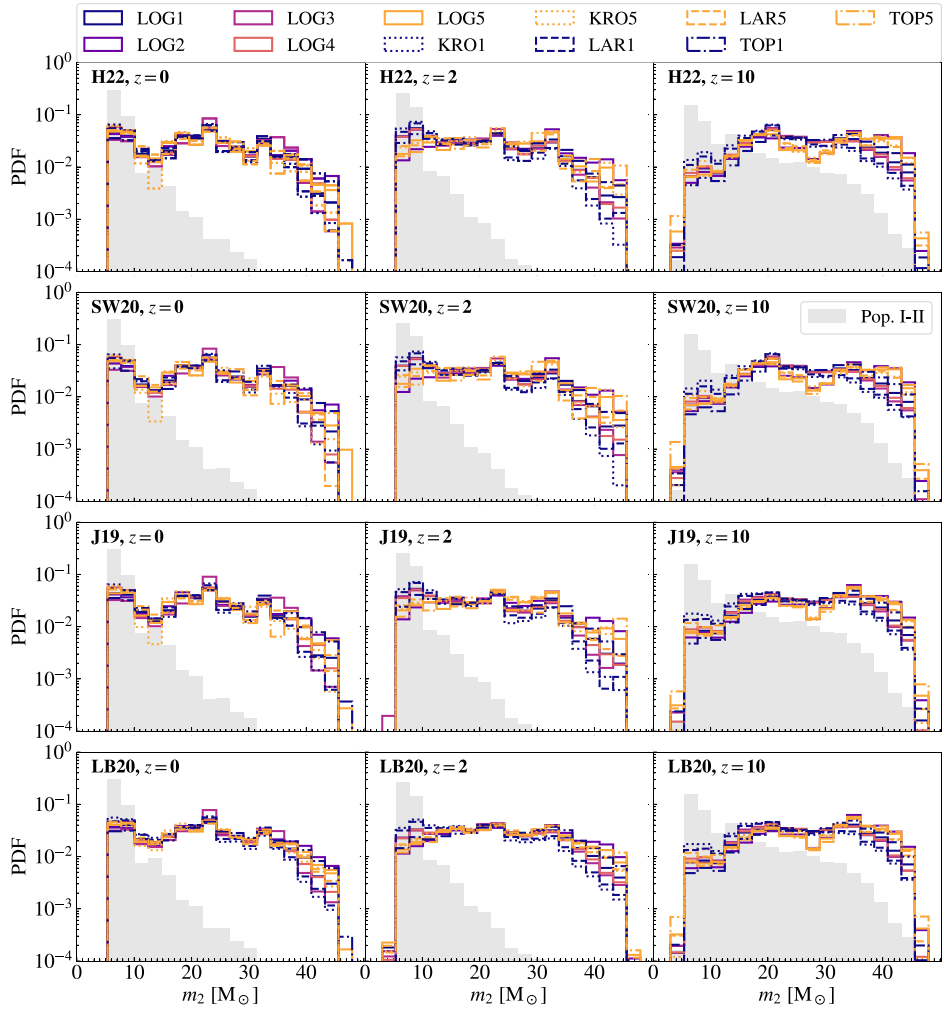

Figure 9. Same as Fig. 8 but for the secondary BH mass m_2.

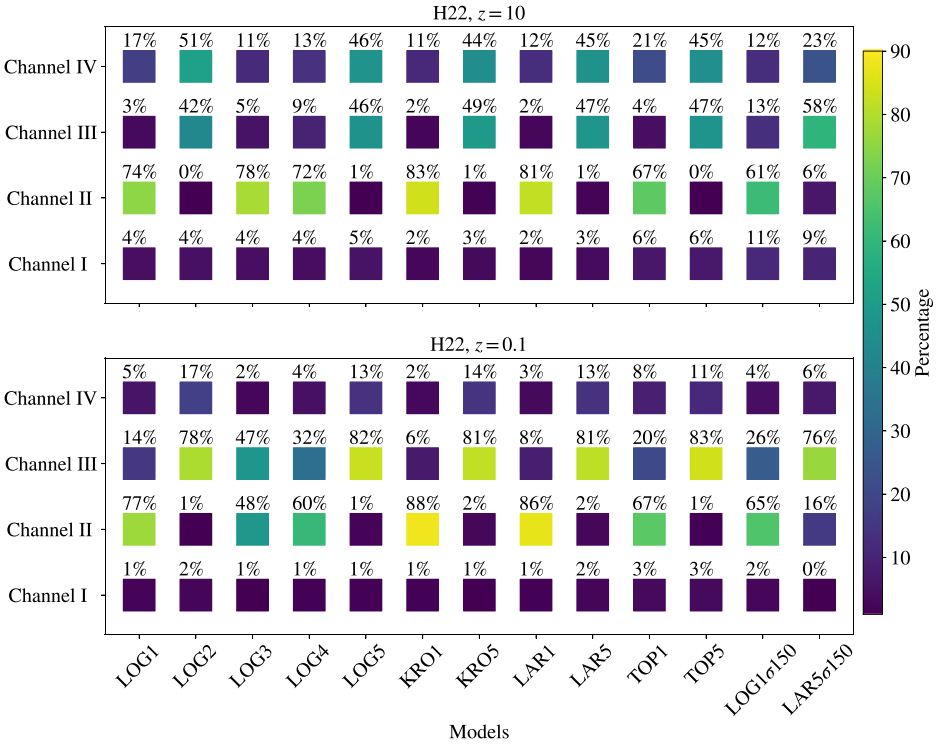

Figure 10. Percentage distribution of formation channels for all the models adopted in this work. Upper (lower) panel: Pop. III BBHs that merge at $z = 10$ ($z = 0.1$). Channel I includes all the systems that undergo a stable mass transfer before the first BH forms, and later evolve through at least one common-envelope phase. Channel II encompasses systems that interact only via stable mass transfer (no common envelopes). Channels III and IV consist in systems that experience at least one common envelope before the formation of the first BH. The only difference between them is that one of the two stars retains a fraction of its H-rich envelope until the formation of the first BH in channel III, while both stars have lost their envelope by the formation of the first BH in channel IV.

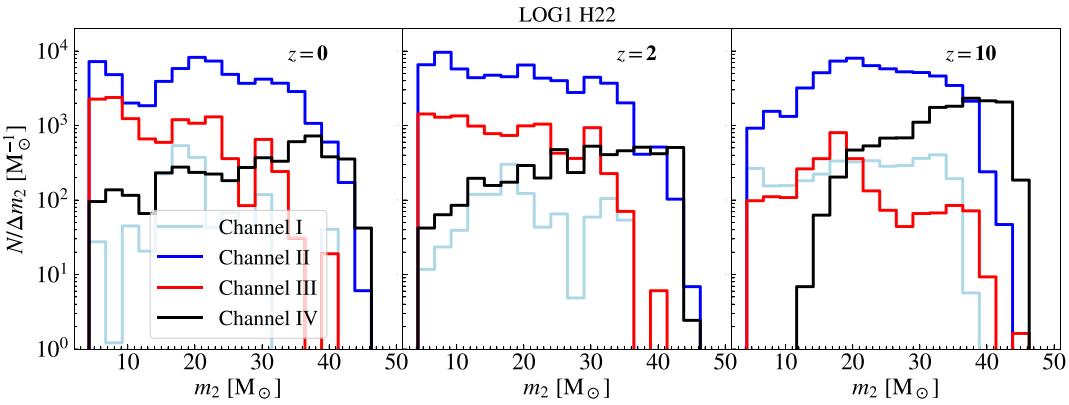

Figure 12. Secondary BH mass distribution m_2 for three different redshift bins (from left to right: $z = 0$, 2, and 10). We show model LOG1 with the H22 SFRD. Light-blue line: channel I; blue line: channel II; red line: channel III; black line: channel IV.

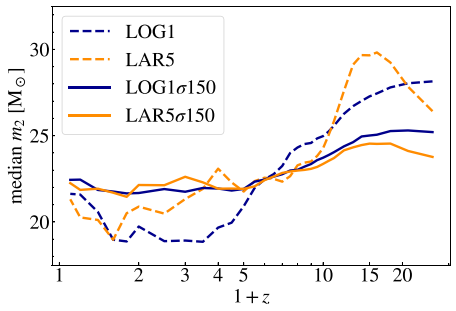

Figure 13. Evolution of the median secondary BH mass m_2 as a function of redshift, for LOG1 and LAR5, with the H22 star formation rate. Solid (dashed) line: natal kicks drawn from model σ150 (GM20).

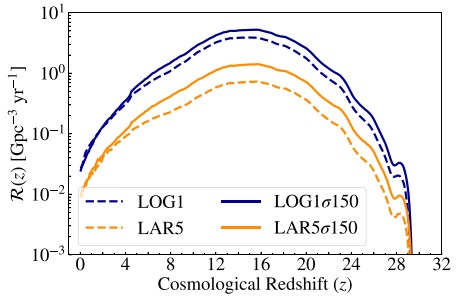

Figure 14. Evolution of the merger rate density with redshift $\mathcal{R}(z)$ for LOG1 and LAR5, with the H22 star formation rate. Solid (dashed) line: natal kicks from model σ150 (GM20).

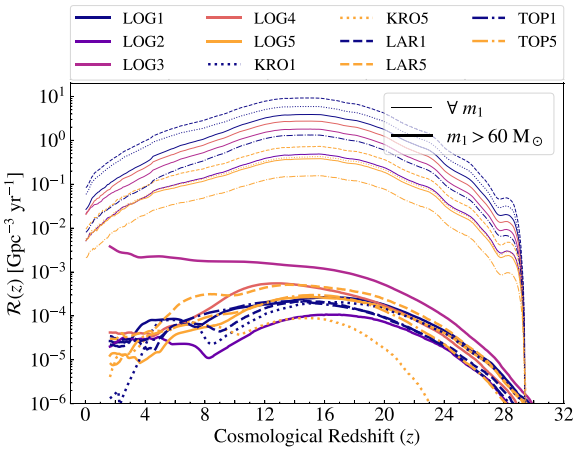

Figure 15. The thick lines show the merger rate density evolution of Pop. III BBHs with primary BH mass $m_1 > 60$ M$_\odot$. For comparison, the thin lines show the total merger rate density evolution of Pop. III BBHs (for any value of m_1). For all the models in this Figure, we use the Pop. III star SFRD from H22 (fig. 1). The colours and line types refer to different initial orbital parameters (table 1).

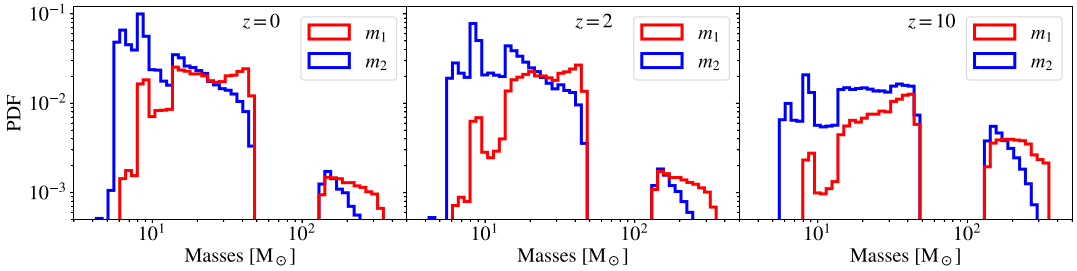

Figure 17. Primary BH mass (red) and secondary BH mass (blue) of Pop. III BBHs merging at redshift $z = 0$, (left), 2 (middle), and 10 (right) assuming the star formation history from H22 and the initial binary orbital parameters as in model LOG1 (table 1). Here, we evolve pure-helium stars.

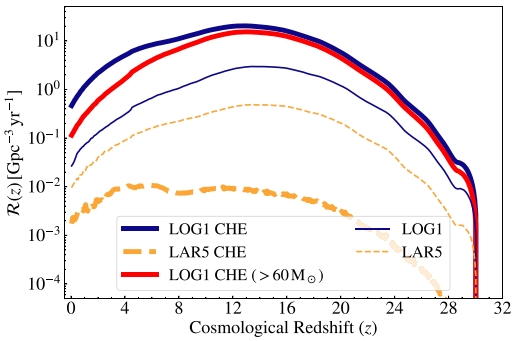

Figure 18. Merger rate density of Pop. III BBHs born from pure-helium binary stars assuming the star formation history from H22. Thick solid blue line: pure-helium binary stars evolved with LOG1 initial conditions. Thick solid red line: we show only the merger rate density of BBHs with primary mass >60 M$_\odot$ for pure-helium binary stars evolved with LOG1 initial conditions. Thick dashed orange line: pure-helium binary stars evolved with LAR5 initial conditions. Thin solid blue (Thin dashed orange) line: model LOG1 (LAR5) with pure-hydrogen binary stars for comparison.

DATA AVAILABILITY

The main data presented in this work are publicly available on Zenodo at Santoliquido (2023). The latest public version of SEVN can be downloaded from this repository.[1] COSMO$\mathcal{R}$ATE is publicly available on GitLab at this link.[2] Further data and codes will be shared on reasonable request to the corresponding authors.

REFERENCES

Giacobbo N., Mapelli M., 2020, ApJ, 891, 141 (GM20)
Hartwig T. et al., 2022, ApJ, 936, 45 (H22)
Hurley J. R., Tout C. A., Pols O. R., 2002, MNRAS, 329, 897
Jaacks J., Finkelstein S. L., Bromm V., 2019, MNRAS, 488, 2202 (J19)
Liu B., Bromm V., 2020, MNRAS, 497, 2839 (LB20)
Santoliquido F., 2023, Binary black hole mergers from Population III stars: uncertainties from star formation and binary star properties. Available at: https://doi.org/10.5281/zenodo.10256327
Skinner D., Wise J. H., 2020, MNRAS, 492, 4386 (SW20)

APPENDIX B

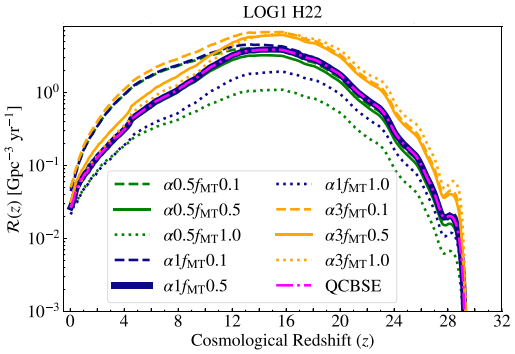

Figure B1. BBH Merger rate density evolution assuming the star formation rate history from H22 and the initial binary orbital parameters as in model LOG1 (table 1). Dashed, solid, and dotted lines refer to models with mass-accretion efficiency $f_{\rm MT} = 0.1$, 0.5, and 1, respectively. Green, blue, and yellow lines refer to models with $\alpha = 0.5$, 1 and 3, respectively. The thick solid blue line (with $f_{\rm MT} = 0.5$ and $\alpha = 1$) is the same as model LOG1 (solid blue line) in Fig. 2. Finally, the dot–dashed magenta line (model QCBSE) is the same as the solid blue line but adopts the mass-transfer stability criteria by Hurley, Tout & Pols (2002).

[1] https://gitlab.com/sevncodes/sevn.git
[2] https://gitlab.com/Filippo.santoliquido/cosmo_rate_public

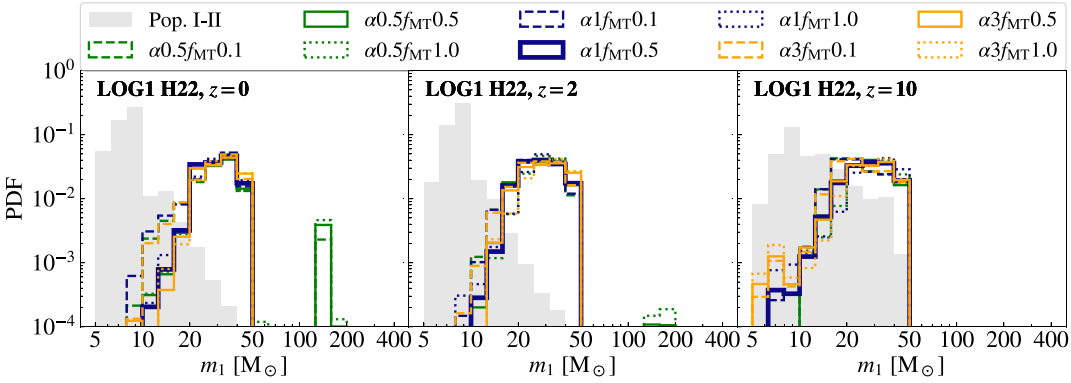

Figure B2. Primary BH mass distribution of Pop. III BBHs merging at redshift $z = 0$, (left), 2 (middle), and 10 (right) assuming the star formation history from H22 and the initial binary orbital parameters as in model LOG1 (table 1). Dashed, solid, and dotted lines refer to models with mass-accretion efficiency $f_{\rm MT} = 0.1$, 0.5, and 1, respectively. Green, blue, and yellow lines refer to models with $\alpha = 0.5$, 1, and 3, respectively. The grey shaded histogram shows the distribution of Pop. I–II BHs for comparison. The model QCBSE (magenta line in Fig. B1) is not shown here, because it perfectly overlaps with model LOG1 (thick solid blue line).

This paper has been typeset from a TEX/LATEX file prepared by the author.